

# Optimization of custom cementless stem using finite element analysis and elastic modulus distribution for reducing stress-shielding effect

Gurunathan Saravana Kumar<sup>1</sup> and Subin Philip George<sup>2</sup>

## Abstract

This work proposes a methodology involving stiffness optimization for subject-specific cementless hip implant design based on finite element analysis for reducing stress-shielding effect. To assess the change in the stress-strain state of the femur and the resulting stress-shielding effect due to insertion of the implant, a finite element analysis of the resected femur with implant assembly is carried out for a clinically relevant loading condition. Selecting the von Mises stress as the criterion for discriminating regions for elastic modulus difference, a stiffness minimization method was employed by varying the elastic modulus distribution in custom implant stem. The stiffness minimization problem is formulated as material distribution problem without explicitly penalizing partial volume elements. This formulation enables designs that could be fabricated using additive manufacturing to make porous implant with varying levels of porosity. Stress-shielding effect, measured as difference between the von Mises stress in the intact and implanted femur, decreased as the elastic modulus distribution is optimized.

## Keywords

Stress shielding, femur, custom implant, elastic modulus distribution, cementless hip implant, finite element analysis, optimization

Date received: 10 February 2016; accepted: 4 December 2016

## Introduction

Cementless femoral stems have been used in preference to cemented stems in total hip replacements (THR) due to prevalence of failure of interfacial cement and large bone loss during surgery in the case of the later.<sup>1,2</sup> One of the predominant modes of failure of cementless prosthesis is long-term aseptic loosening of artificial joint components in bone.<sup>3</sup> The main cause for this is due to the unnatural stress distribution in the bone caused by the load transfer between a stiff implant and relatively flexible bone, and the resulting stress-shielding effect,<sup>4</sup> followed by bone resorption in areas of the bone-implant interface. Another major failure mode is debonding at interface caused by relative micro motions due to improper implant fitting in the bone cavity.<sup>3</sup>

Thus, to avoid the failures, the main contributing factors, that is, stress and motions in bone and implant that depend mainly on loading conditions and on the implant design, that is, its mechanical properties and geometry have to be considered. Custom prostheses have gained a lot of popularity in today's world owing

to its adaptability in form and fit to the anatomy of the patient. They are usually designed pre-operatively using computed tomography (CT) data.<sup>5,6</sup> The earliest attempt to produce customized implant employing a computer-aided design (CAD) system taking CT data as input was made by Viceconti et al.<sup>7</sup> The study by Kawate et al.<sup>8</sup> reports that customized implant design provides appreciable results for patients whose femurs have significant anatomical deformity. In a related work, the authors have reported a parametric CAD framework for custom implant design.<sup>9</sup> However, in all these studies, the main objective has been to create implant stem profiles with good fit and fill

<sup>1</sup>Department of Engineering Design, Indian Institute of Technology Madras, Chennai, India

<sup>2</sup>Department of Mechanical Engineering, Amal Jyothi College of Engineering, Kottayam, India

## Corresponding author:

Gurunathan Saravana Kumar, Department of Engineering Design, Indian Institute of Technology Madras, Chennai 600036, India.  
 Email: [gssarvana@iitm.ac.in](mailto:gssarvana@iitm.ac.in)

characteristics and the same has been demonstrated with no reports of analysis of stress shielding in the femur accompanied by these design. When the metallic prosthesis (with higher stiffness than the bone) is introduced into the femur, it alters the physiological stress distribution and induces stress shielding and bone atrophy<sup>10</sup> and results in implant loosening. This had led to research in using flexible implants (with low stiffness) to reduce stress-shielding effect, but a flexible implant may produce higher stresses along the interface.<sup>10</sup> A design scheme which considers both interface failure as well as bone loss due to stress shielding has been proposed using optimization of non-homogeneous elastic modulus distribution.<sup>11</sup>

However, it is imperative that advances in developing subject-specific three-dimensional (3D) bone-implant finite element (FE) models that are capable of predicting fully 3D stress states accompanied by simulations, accurately capturing the physiological loading will be necessary for effective optimization of stem designs. A recent work reports employing heterogeneous material distribution in cementless stem for design optimization considering stress-shielding effect.<sup>11</sup> The CAD framework for custom implant design developed by the authors<sup>9,12</sup> has resulted in stem designs with superior fit and fill with bone, as compared to a commercial modular implant.<sup>12</sup> A fully 3D stress state analysis using a simplified loading showed that the custom implant causes less stress shielding in the proximal femur.

This work envisages a FE-based design optimization scheme where the femoral stem elastic modulus distribution is optimized over the stem volume. The objective of the optimization, subject to constraints is to reduce stress-shielding effect by providing stress as close as possible to physiological levels in the proximal femur

regions. The optimization problem formulation for stress shielding in this work differs from the formulation of the problem by Fraldi et al.,<sup>11</sup> where topology optimization is used to minimize the mass of the stem. In that work, the preference is to have either solid elements or empty elements and explicitly penalize grey elements to limit their presence in the final solution. This formulation enables realizing the optimized design by introducing holes being drilled in locations of empty elements.<sup>11</sup> On the contrary, in this work the problem is formulated as material distribution problem and grey elements (i.e. elements with density in between 0 and 1) are not penalized. In fact, the elements with grey level are preferred. This is because the fabrication method envisaged for such structures is to use additive manufacturing techniques which can enable fabrication of porous structures with varying levels of porosity for orthopaedic applications.<sup>13,14</sup> The article describes the formulation, the numerical methods and analysis techniques employed and the outcomes of the work.

## Methodology

Figure 1 schematically illustrates the complete methodology for custom cementless stem design to obtain prosthetic stem profile for good form fit and elastic modulus optimization for reducing the stress-shielding effect. The methodology involves two phases. The initial phase consists of subject-specific 3D reconstruction of femur geometry and extraction of a set of pre-specified femoral features that are used for generating custom implant stem profile. A CAD model of the same is automatically instantiated from the parametric model using the developed libraries and associated interface. The details of these methodologies are described in previous publications by the present authors.<sup>9,12</sup> In phase 2,

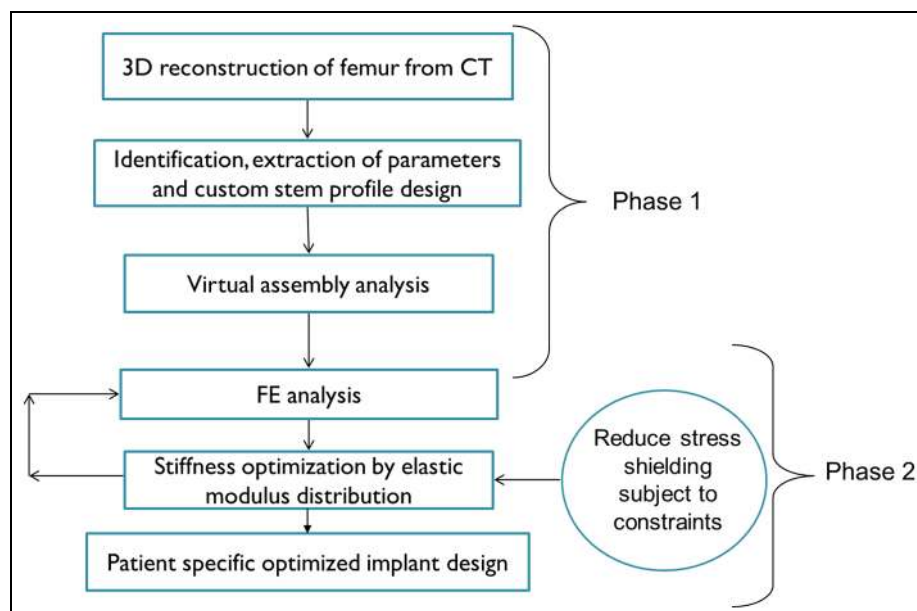


**Figure 1.** Schematic diagram of the proposed methodology.

the main focus of this article, initial FE analysis with faithful reproductions of actual geometries of the bone and implant and accurate mechanical properties of the materials involved in the analyses with physiological boundary conditions were used to ascertain stress-shielding effect caused due to insertion of the designed implant. A commercially used modular implant design chosen for the comparison of form fit in the earlier work<sup>12</sup> was used for comparing the stress-shielding effect, and it was shown that the custom implant designed using the proposed design methodology fared well in terms of stress-shielding effect. In this work, FE-based optimization is done to reduce stress-shielding effect by reducing the implant stiffness by appropriate elastic modulus distribution subject to constraints like implant failure and limiting stresses at the bone-implant interface. The details of the methodology are described in subsequent sections.

### *FE analysis of bone-implant model*

The mechanical response of the resected human femur with implant is assessed non-invasively using FE analysis. As the mechanical properties of femoral bone vary with the individual and the location,<sup>15</sup> in this work the mechanical properties of the femur are subject- and site specifically assigned. The generation of the FE models of the femur from the CT data set is similar to the method described in detail by Taddei et al.<sup>16</sup> The CT data sets were read in Amira® and segmented for model generation and exported to Abaqus®. C3D4 tetrahedral elements were used for meshing as they yield a good geometrical fit with medical mesh models. The femur model is resected, and the implant stem is assembled. The assembly is simulated for combined loading simulating simultaneous single-leg stance and stair climbing. The hip joint loading during all other common activities of most hip patients are comparably small (except during stumbling), thus implants should mainly be tested with loading conditions that mimic walking and stair climbing.<sup>17</sup> A load jig simulating very closely this physiological loading on the bone-implant assembly<sup>18</sup> is used for the present optimization framework. The FE model simulating this physiological loading is shown in Figure 2. To simulate this loading, the femur is tilted to 12° in valgus, and the distal end is constrained, allowing it only to rotate around its own axis. An axial load acts at the end of a lever arm (simulating pelvis beam) along the vertical axis (pubic centre line) and a torsional load at the distal end of femur. A pulley system (at C1 and C2) simulates the load between the iliotibial band (C2-C3) and the abductor muscles on the greater trochanter (E to C1). The contact conditions between the implant stem surface and femoral canal surface is formulated as small sliding formulation with friction. The load acting on the jig was given in two steps, initially a vertical load of 600 N was applied at A, and in the second step, a torque load of 10 N m is

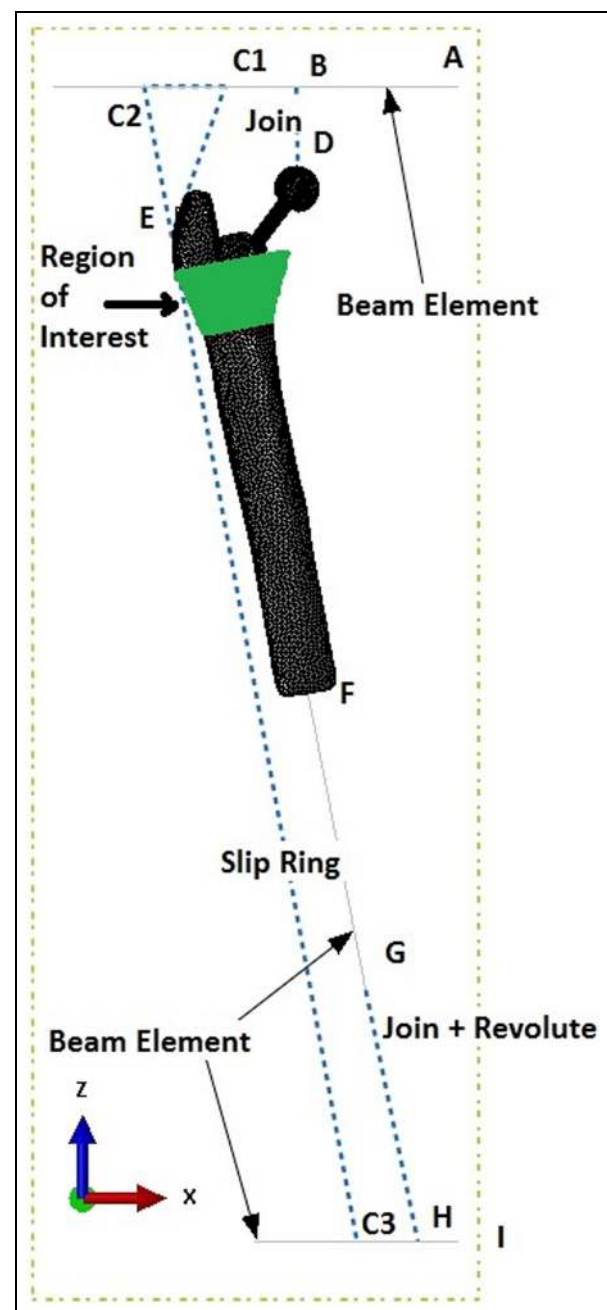


**Figure 2.** FE model of implant–bone assembly with load jig for simulation.

applied at G. These values correspond to the single-leg stance while stair climbing for a body weight of 70 kg.<sup>18</sup>

### *Implant optimization by elastic modulus distribution*

The bone-implant assembly behaves like a composite structure, and based on the principle of Wolff's law, stress shielding occurs in bone when a high-stiffness implant is introduced in it.<sup>10</sup> This ratio of the elastic moduli plays significant role in defining the interfacial shear stress as well as the stress shielding happening in the bone around the prosthesis.<sup>17</sup> FE-based optimization for implant mass reduction and thus lowering the

implant stiffness has shown reduction in stress concentration at the interfaces and the stress shielding in proximal and distal femur regions.<sup>11,19</sup> In these models, either the material is distributed in the given volumetric domain as discrete values (presence/absence of holes) or the material is assumed to have continuous gradation, where the volume fraction distribution in the solid domain establishes a continuous variation of the apparent density. This mass variation (and thus the elastic modulus distribution) is optimized for a design goal and is accomplished by FE model, analysis and associated numerical code. In this work, the later approach, that is, a continuous variation of the apparent density is followed. Note that the external shape of the implant is retained in the optimization process. The continuous variation of apparent density can be physically obtained by fabricating continuously varying porous structures. Porous metallic constructs can be synthesized by sintering technique,<sup>20</sup> and recent advances in additive manufacturing enable construction of continuously varying porous structures in medical grade titanium alloys.<sup>13,14</sup> The mechanical properties of the resultant implant at a specific site in the design volume will depend upon the porosity distribution at that location. Correlation between the mechanical properties (like elastic modulus) and the porosity in titanium alloys are available in the literature,<sup>20</sup> and the same is used in our formulation.

The objective of the optimization is to minimize the deviation of stress-strain state between an intact and operated femur. This deviation can be modelled as stress-shielding increase (SSI) based on the von Mises stress values<sup>11</sup> or von Mises strain values.<sup>18</sup> In this work, SSI is modelled as the relative difference between volume average of the von Mises stress of the intact and the implanted femur calculated over a region of interest (ROI). Since clinical as well as numerical studies have shown that the proximal femur is the most affected region due to stress-shielding effect of cementless implants,<sup>4,21</sup> in this study, the same is considered as the ROI to monitor stress and strain distribution. The ROI is chosen consisting of element set spanning the medial curvature around the lesser Trochanter as shown in Figure 2. Thus, the objective is formulated as

$$\text{Minimize } SSI = \frac{\sigma_{vM}^{\text{pre-THR}} - \sigma_{vM}^{\text{post-THR}}}{\sigma_{vM}^{\text{pre-THR}}} \quad (1)$$

where  $\sigma_{vM}^{\text{pre-THR}}$  is the volume average of von Mises stress for the elements in the ROI for the intact femur,  $\sigma_{vM}^{\text{post-THR}}$  is the volume average of von Mises stress for the elements in the ROI for implanted femur, and the same is computed as,  $\sigma_{vM}^{\text{pre-THR}}$  or  $\sigma_{vM}^{\text{pre-THR}} = \sum \frac{1}{Vol_{\text{element}}} \sum Vol_{\text{element}} \times \sigma_{\text{element}}$  where  $Vol_{\text{element}}$  is elemental volume and  $\sigma_{\text{element}}$  is von Mises stress at the centroid of the element.

This performance increase is subject to various constraints such as the limiting stresses in the implant to

prevent its failure, limiting interfacial stresses in the bone-implant interface and manufacturing constraints on range of volume fractions obtainable (and thus the corresponding stiffness) in the titanium implant constructs by sintering process. These are formulated, respectively, as

$$\begin{aligned} \sigma_{vM}^i &< \sigma_{y-\min}, \quad i = 1, 2, \dots, N \\ \text{Subject to} \quad \tau_{avg}^{\text{interface}} &< \tau_{\max} \\ E_l &\leq E^i \leq E_u \end{aligned} \quad (2)$$

where  $\sigma_{vM}^i$  is the von Mises stress in the implant element set  $i$ ,  $\sigma_{y-\min}$  is the yield stress for implant material corresponding to the highest porosity;  $\tau_{avg}^{\text{interface}}$  is the average interfacial shear stress at implant and femur bone interface,  $\tau_{\max}$  is the maximum allowable value of interfacial shear stress at implant and femur bone interface.  $E_l$  and  $E_u$  are lower and upper limits of Young's modulus, respectively, for the range of porosity considered in implant metal. These lower and upper bounds of Young's modulus determine the termination criteria for the optimization process.

The volume of implant stem that will undergo the elastic modulus optimization is divided into  $N$  element sets.  $N$  can be as large as the number of tetrahedral elements in implant stem, but considering computational expense, a lower value is chosen. The criterion for forming the element set is based on the von Mises stress distribution in the design volume. The complete range of von Mises stress in implant stem is divided into  $N$  intervals, and the element groups are specified using those intervals. The implant stem is assigned the material property of medical grade titanium (Ti-6Al-4V) with isotropic Young's modulus varying as per the volume fraction in the given element set with Poisson's ratio of 0.3. The head and neck regions are not considered for stiffness optimization and only the stem is considered (as shown in Figure 3). The local variation in elastic modulus is assigned to the elements belonging to the stem by considering the relationship between volume fraction and modulus as obtained in sintered titanium with maximum Young's modulus of 110 GPa and as reported by Oh et al.<sup>20</sup> The following relation is used

$$E^i = -2.625 \times (1 - \rho^i) + 110, \quad i = 1, 2, \dots, N \text{ in GPa} \quad (3)$$

where  $\rho^i$  is the volume fraction of material in the elements belonging to the volume of  $i$ th element set. The modulus ( $E^1, E^2, E^3, \dots, E^N$ ) that are assigned to each element set are the design variables.

### Numerical optimization

The topology optimization formulation is typically solved using classical variational approach,<sup>22</sup> with a two-step process in each iteration, computing the displacements for a given element stiffness and then updating the new value of element stiffness by keeping these

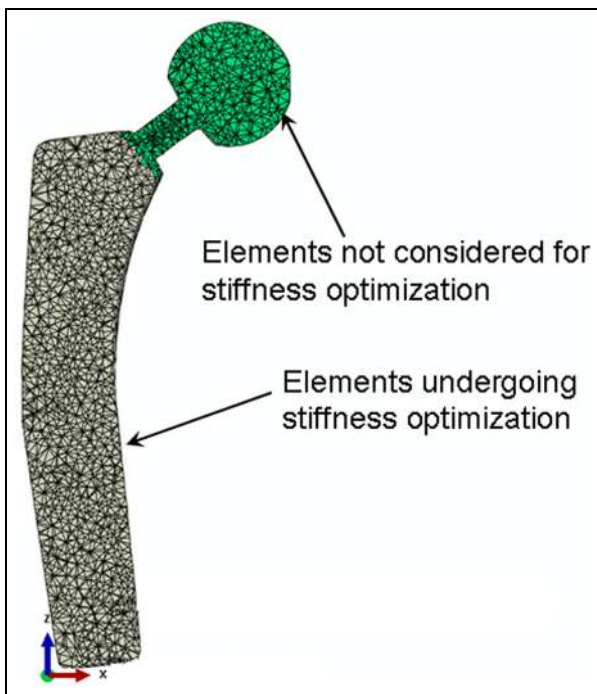


**Figure 3.** Region of custom THR implant considered for stiffness optimization.

nodal displacements constant. The formulation in this work is explicit. The element stiffnesses, which are the variables, are updated using a numerical approach of finding their sensitivity to SSI.

The algorithm used in the optimization process is shown in Figure 4(a), and the same is coded as application programming using Python in Abaqus. The numerical optimization method employed in the work is steepest descent method, and the gradients for objective function are evaluated using forward difference method. The FE models for the femur-implant assembly and the intact femur in the load jig are simulated as described in section ‘FE analysis of bone-implant model’ for each function evaluation, that is, to compute the SSI. The design volume considered for elastic modulus optimization (which is the stem region of the implant as shown in Figure 3) is divided into  $N$  element groups with material properties corresponding to the porosity in that particular element set as described in section ‘Implant optimization by elastic modulus distribution’. Figure 4(b) shows the cross section of an implant with  $N$  material property gradation. The volume average of von Mises stress distribution in the ROI is computed for the intact FE model and the model assembled with bone and implant for small perturbations ( $\Delta E^i$ ) in all the components of the design variables ( $E^1, E^2, E^3, \dots, E^N$ ). The change in SSI corresponding to each design variables are computed as

$$\frac{\partial(\text{SSI})}{\partial(E_i)} = \frac{f(E^1, E^i + \Delta E^i, E^{i+1}, E^N) - f(E^1, E^i, E^{i+1}, E^N)}{\Delta E^i} \quad (4)$$

where  $\Delta E^i$  is the small perturbation in individual material property (Young’s modulus). For this work, the same is taken as 1% of Young’s modulus. If the objective function (SSI) reduces, then constraint violations and termination criteria are checked. If both the conditions are satisfied, then the algorithm proceeds to the next iteration, with the design variables as

$$E^{n+1} = E^n + \alpha \times \frac{\partial(\text{SSI})}{\partial(E_i)} \quad (5)$$

where  $\alpha$  is the step length and its initial value is chosen as  $1 \times 10^{-10}$  for this work. If the objective function does not reduce, then the design variables are recomputed by increasing  $\alpha$  and using the same set of gradients. The iterations are continued until the termination criteria are met. The method is computationally stable and guarantees solution improvements with each iteration, but the limitation is that the search will slow down with reduction in magnitude of the gradient vector. In an engineering problem like the one solved here, with active constraints this is not a serious limitation since objective function gradients do not vanish at optimal solution point.

## Results and discussions

To demonstrate and validate the methodology of optimizing the implant stem, six sample CT data of adult Indian male femur taken in vivo were used. Hereafter in the study, they will be indexed and referred to as S1, S2, ..., S6. The femur geometry was reconstructed, and feature extraction was done for six custom implant designs. The six custom implant models were generated and then fitted into the reconstructed specimens of femur. The FE analysis simulating simultaneous single-leg stance and stair climbing was performed and the stress-strain state of the femur and the implant were analysed. Maximum von Mises stress for the bone-implant assembly for the six specimens are tabulated in Table 1. These values for the implant as well as the femur are in the allowable range.<sup>21</sup> The optimization considering the elastic modulus distribution was employed with number of element sets ( $N$ ) as 10 to limit the computational expense. The lower and upper limits of stiffness values  $E_l$  and  $E_u$  were taken as 40 and 110 GPa, respectively, corresponding to volume fractions of 0.75 (25% porous) and 1 (completely solid) medical grade titanium alloy.<sup>20</sup> The yield stress for implant metal corresponding to highest porosity, that is, 25% is 40 MPa,<sup>20</sup> and the same is taken as the value for  $\sigma_{y-\min}$ . The maximum interfacial limiting stress  $\tau_{\max}$  is fixed as 3 MPa as this is the reported limiting value of interfacial stress that promotes bone ingrowth at the interface.<sup>23</sup> The numerical optimization code was run in Abaqus, and convergence was obtained for all the six femur specimens considered.

The results of minimizing the SSI by optimization involving elastic modulus distribution with the aim of

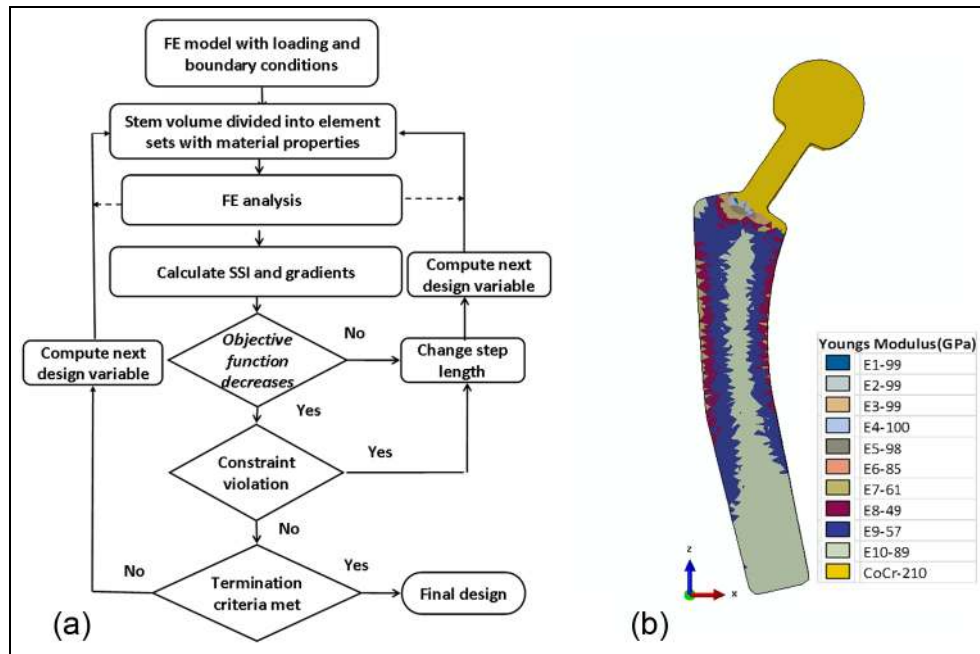


**Figure 4.** (a) Flow chart of the stiffness optimization of custom implant stem and (b) cross section of a stiffness-optimized implant with elastic modulus distribution.

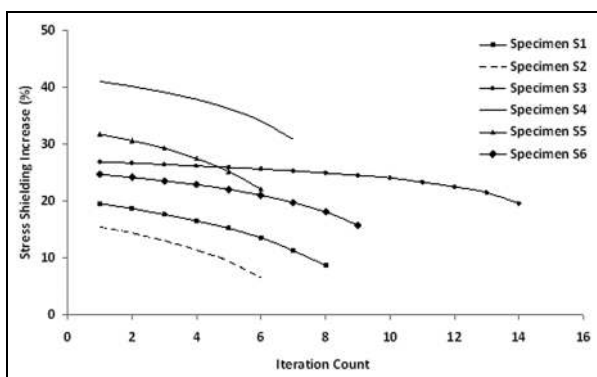


**Figure 5.** Decrease in stress shielding with iterations of numerical optimization of elastic modulus distribution in custom implant.

**Table I.** Maximum von Mises stress in implant–bone assembly.

Specimen no.	Maximum von Mises stress (MPa)	
	Implant	Femur
S1	468	92
S2	381	31
S3	402	61
S4	392	62
S5	338	73
S6	352	58

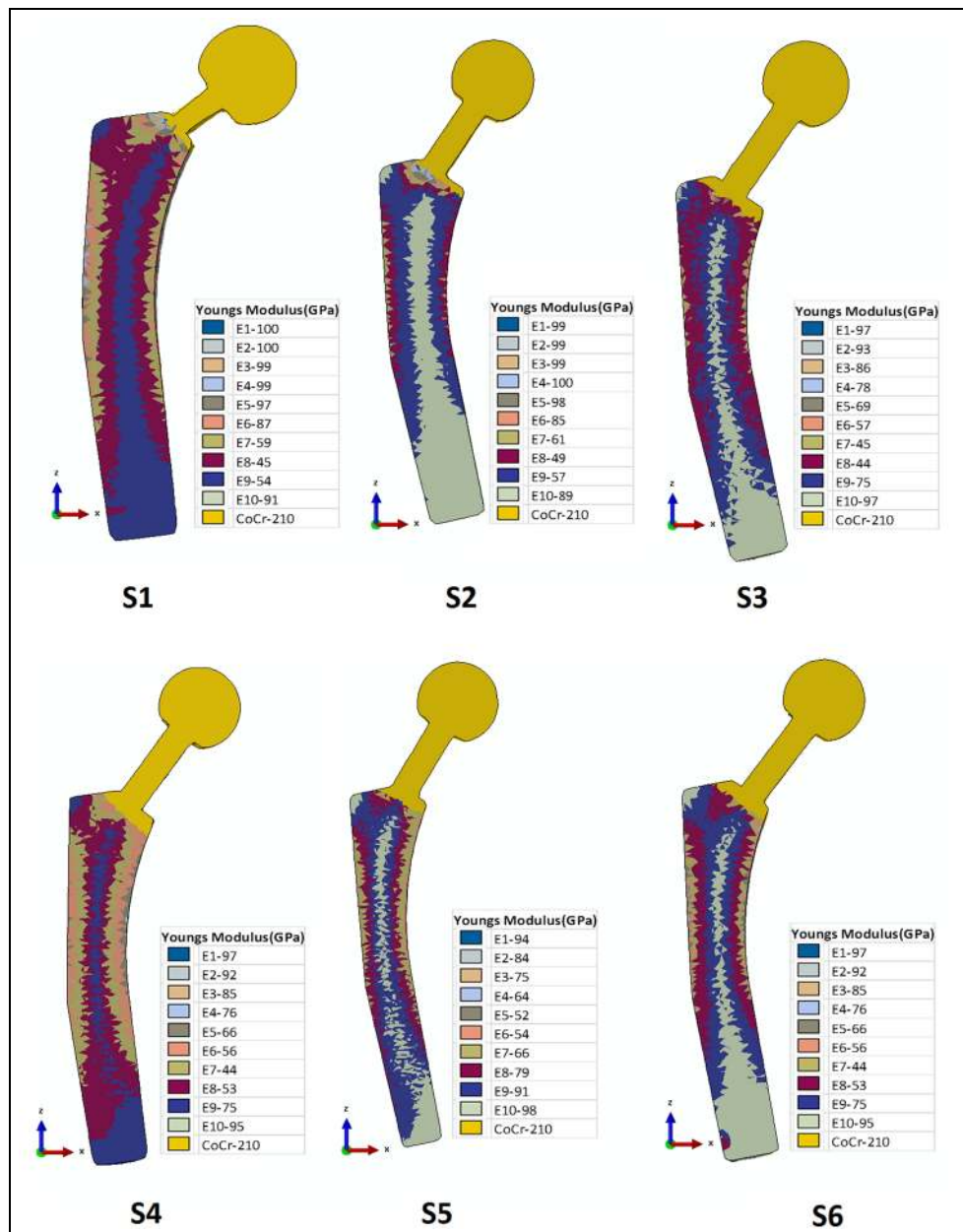
reducing stress-shielding effect has shown positive results for all the six samples considered for the study. Increase in SSI, measured as a ratio between the difference of von Mises stress in the intact and implanted

femur and von Mises stress within the intact femur, computed as an average measure over the volume of elements in ROI show a continuous decrease as the optimization iteration proceed (shown in Figure 5). The decrease in SSI ranges from 7% to 11% for the six specimens (Table 2). The variation in initial SSI among the specimens can be attributed to the difference in geometry of the custom implants and thus the volume of bone is removed due to implant fixation. Complete reduction in stress-shielding effect could not be obtained, owing to constraints put forth by the limiting values of interfacial shear stress and the lower bound of stiffness. The interfacial shear stresses were always within the limits throughout the iterations (Table 2). In all the optimization runs, the exit criteria for optimization was reaching the lower bound of stiffness  $E_l$ , thus suggesting that a relaxation on this value can lead to further reduction in SSI. This value can be relaxed if possibilities of obtaining higher porosities in sintered titanium constructs without very low failure stresses are proven feasible by research. Figure 6 shows the result of the optimization in terms of the resulting elastic modulus distribution for all<sup>24</sup> the six implants, and the corresponding von Mises stress distribution for the femur–implant assembly is shown in Figure 7. The mass reduction in percentage, after optimization of the six specimens, is presented in Table 3. It is seen that more than 10% of the weight of the solid implant was reduced with optimization in all the six cases.

In order to evaluate the performance of the optimization in custom implant, the effective strain is monitored in the ROI to study the stress-shielding effect and resulting bone loss. This is studied using the ‘mechanostat’ theory proposed by Frost.<sup>25</sup> A window of

**Table 2.** Decrease in stress-shielding increase with implant stiffness optimization.

Specimen no.	Stress-shielding increase (SSI) (%)			Average interfacial shear stress after optimization ( $\tau_{avg}^{interface}$ ) (MPa)
	Before optimization	After optimization	Change	
S1	19.47	8.62	10.85	2.36
S2	15.4	6.42	9	1.66
S3	26.83	19.5	7.33	2.94
S4	41	30.8	10.2	2.32
S5	31.75	22	9.71	2.39
S6	24.6	15.7	8.9	1.42

**Figure 6.** Stiffness-optimized custom implants showing elastic modulus distribution for six femur specimens.

mechanical usage is considered as physiological that keeps a normal balance between bone formation and

resorption. The boundary of this window is defined using effective strain<sup>24</sup> defined as

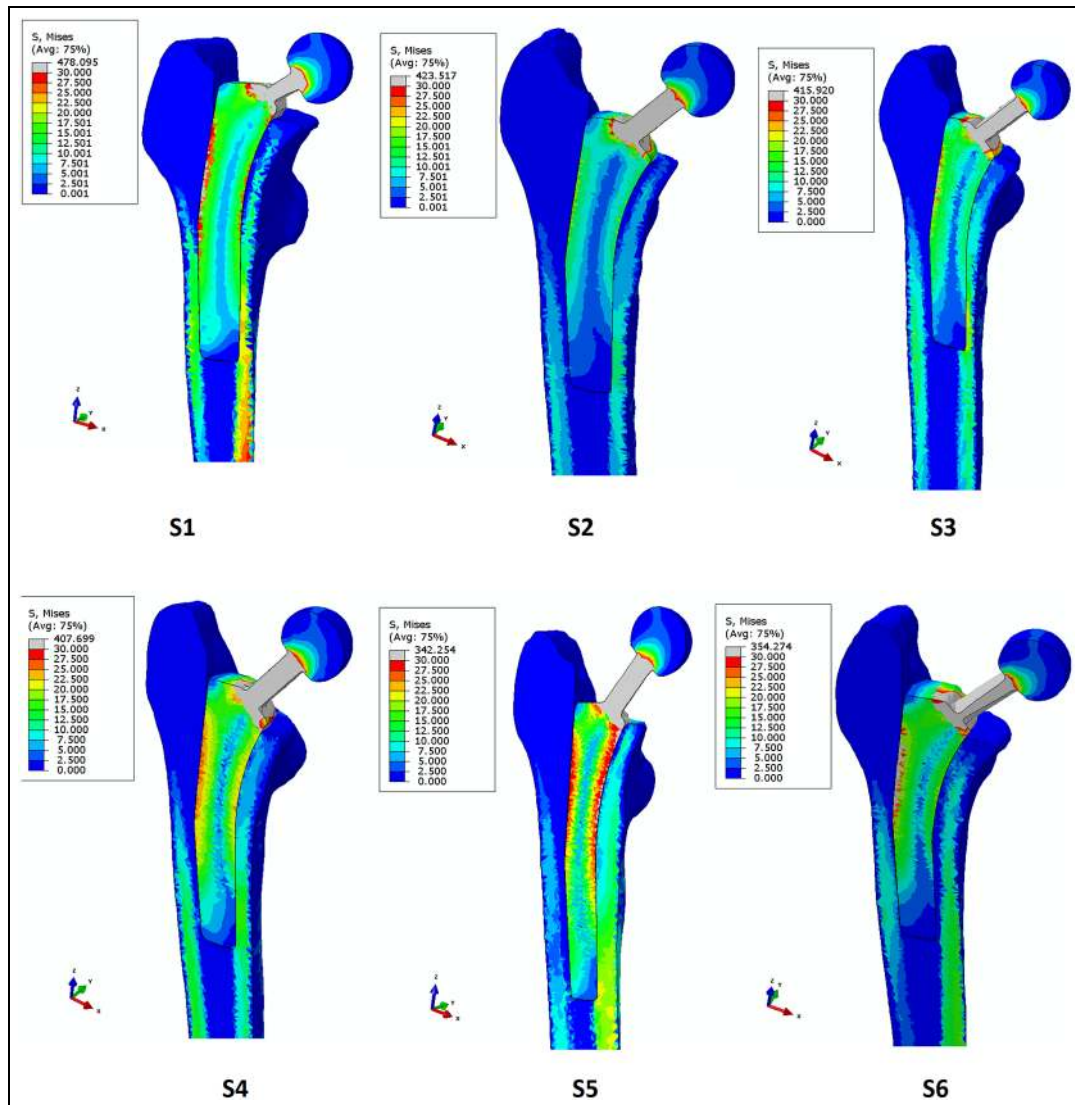


**Figure 7.** von Mises stresses in implant–bone assembly for the stiffness-optimized custom implants for six femur specimens.

**Table 3.** Mass reduction in percentage for six specimens after stiffness optimization.

Specimen no.	Mass reduction (%)
S1	16.10
S2	14.46
S3	13.63
S4	11.50
S5	11.05
S6	14.45

$$\varepsilon = \sqrt{\frac{1}{2}((\varepsilon_1 - \varepsilon_2)^2 + (\varepsilon_2 - \varepsilon_3)^2 + (\varepsilon_3 - \varepsilon_1)^2))} \quad (6)$$

where  $\varepsilon_1$ ,  $\varepsilon_2$  and  $\varepsilon_3$  are the principal strains. The strain range that promotes bone growth is between 1000 and 4000  $\mu$ -strain.<sup>26</sup> The effective strain histograms were plotted for the elements in the ROI for the intact bone, bone loaded by custom implant with full elastic modulus (110 GPa) throughout and the bone loaded by custom

implant with optimized elastic modulus distribution. The strain histograms plotted using a 100  $\mu$ -strain window for all the six specimens considered for the study are shown in Figure 8. The histograms show that a greater number of elements or equivalent volume fraction of the femur bone in the ROI is maintained in the physiological window of strain, that is, between 1000 and 4000  $\mu$ -strain in the femur introduced with the custom implant with optimized elastic modulus distribution. Note the shift of the peak value of histogram towards physiological window of strain for the bone introduced with optimized custom implant in Figure 8. Thus, the proximal bone loss will be comparatively less for the bone introduced with stiffness-optimized custom implant proposed in this work over the ones without this customization as well as stiffness optimization.

This work is similar to the THR stem optimization presented by Fraldi et al.,<sup>11</sup> in the sense both the works aim at reducing SSI caused by the introduction of implant, but our work differs in the methodology as well as the outcomes. The stiffness minimization

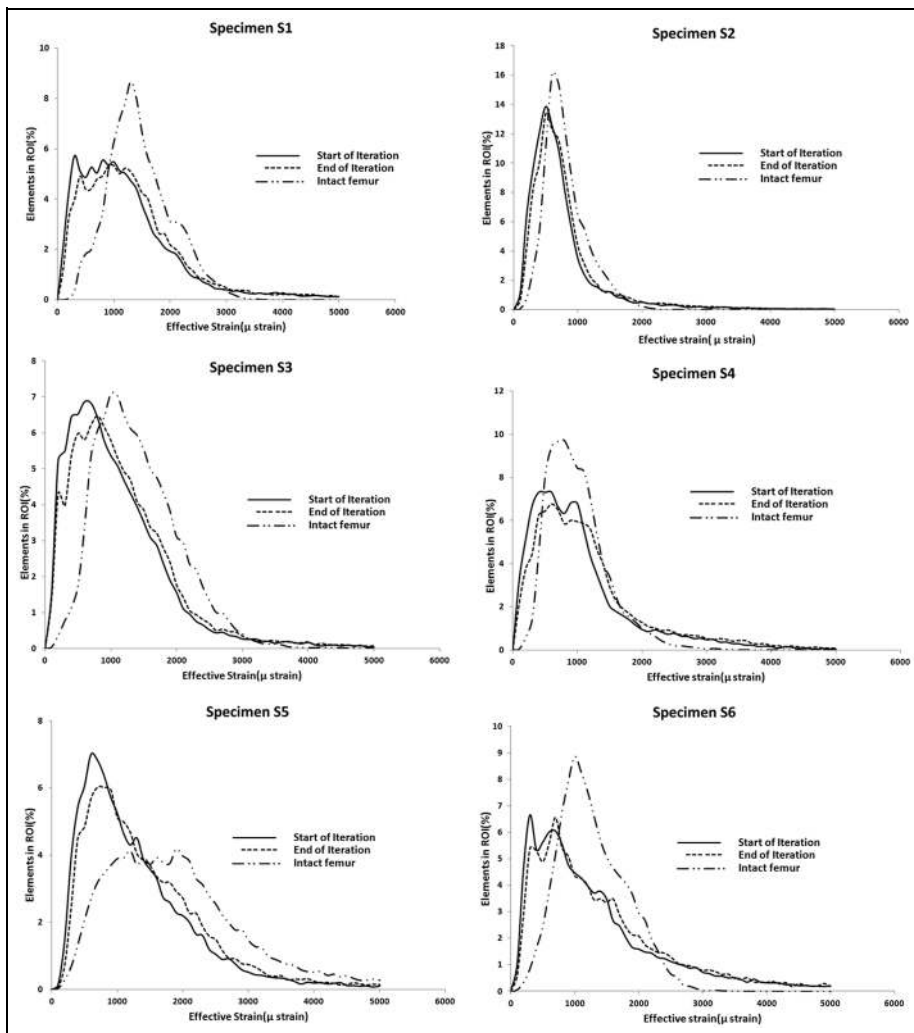


**Figure 8.** Effective strain histograms in ROI for intact femur bone, bone–implant assembly before and after stiffness optimization in the custom implants.

problem is formulated as material distribution problem in this work without explicitly penalizing the presence of partially filled elements, which is not the case in the method employed by Fraldi et al.<sup>11</sup> The final result of such a method is implant stems that are hollow in the centre with steep material density gradients to the outer surface. Whereas, in the design outcome of the proposed procedure are implant stems that have more uniform material gradation. The present formulation enables fabrication of these designs using additive manufacturing of porous structures with varying levels of porosity.

## Conclusion

A methodology involving elastic modulus distribution optimization for custom THR implant stem for possible re-design and analysis specific to patients with the aim of reducing the stress-shielding effect has been proposed and implemented. A detailed FE model based on 3D reconstruction and bone material properties assignment based on CT data was employed. A physiological loading condition was chosen to closely replicate the combined single-leg stance and stair-climbing loading

that are clinically significant. Six sample CT data were used to demonstrate and validate the methodology. The implant stem is optimized using a stiffness optimization involving elastic modulus distribution with an aim to reduce the SSI due to introduction of implant. The decrease in SSI is between 7% and 11%, and further reduction in stress shielding is limited by constraints put forth by the limiting values of interfacial shear stress and the lower bound of stiffness in implant stem. The optimized stem also maintains more regions of the proximal femur around the stem in physiological window of effective strain that promotes bone growth. The authors believe that the inferences from this study can pave ways to optimally design custom implants and utilize advanced manufacturing techniques like additive manufacturing to fabricate porous implants with better prospective.

## Declaration of Conflicting Interests

The author(s) declared no potential conflicts of interest with respect to the research, authorship and/or publication of this article.

## Funding

The author(s) received no financial support for the research, authorship and/or publication of this article.

## References

1. Beckenbaugh RD and Ilstrup DM. Total hip arthroplasty. *J Bone Joint Surg Am* 1978; 60: 306–313.
2. Stauffer R. Ten-year follow-up study of total hip replacement. *J Bone Joint Surg Am* 1982; 64: 983–990.
3. Huiskes R and Verdonschot N. Biomechanics of artificial joints: the hip. In: Mow VC and Hayes WC (eds) *Basic orthopaedic biomechanics*. Philadelphia, PA: Lippincott-Raven, 1997, pp.395–461.
4. Cristofolini L. A critical analysis of stress shielding evaluation of hip prostheses. *Crit Rev Biomed Eng* 1997; 25: 409–483.
5. Reuben JD, Chang CH, Akin JE, et al. A knowledge-based computer-aided design and manufacturing system for total hip replacement. *Clin Orthop Relat Res* 1992; 48–56.
6. Huo MH, Salvati EA, Lieberman JR, et al. Custom-designed femoral prostheses in total hip arthroplasty done with cement for severe dysplasia of the hip. *J Bone Joint Surg Am* 1993; 75: 1497–1504.
7. Viceconti M, Testi D, Gori R, et al. HIDE: a new hybrid environment for the design of custom-made hip prosthesis. *Comput Meth Prog Bio* 2001; 64: 137–144.
8. Kawate K, Ohneda Y, Ohmura T, et al. Computed tomography-based custom-made stem for dysplastic hips in Japanese patients. *J Arthroplasty* 2009; 24: 65–70.
9. Saravana Kumar G and Gupta M. Patient specific parametric geometric modelling of cementless hip prosthesis. In: *Proceedings of the 5th international conference on advanced research in virtual and rapid prototyping*, Leiria, 28 September–1 October 2011. CRC Press.
10. Huiskes R, Weinans H and van Rietbergen B. The relationship between stress shielding and bone resorption around total hip stems and the effects of flexible materials. *Clin Orthop Relat Res* 1992; 274: 124–134.
11. Fraldi M, Esposito L, Perrella G, et al. Topological optimization in hip prosthesis design. *Biomech Model Mechanobiol* 2010; 9: 389–402.
12. George SP and Saravana Kumar G. Patient specific parametric geometric modelling and finite element analysis of cementless hip prosthesis. *Virtual Phys Prototyp* 2013; 8: 1–19.
13. Krishna BV, Bose S and Bandyopadhyay A. Low stiffness porous Ti structures for load-bearing implants. *Acta Biomater* 2007; 3: 997–1006.
14. Mullen L, Stamp RC, Brooks WK, et al. Selective Laser Melting: a regular unit cell approach for the manufacture of porous, titanium, bone in-growth constructs, suitable for orthopaedic applications. *J Biomed Mater Res B Appl Biomater* 2009; 89: 325–334.
15. Cuppone M, Seedhom BB, Berry E, et al. The longitudinal Young's modulus of cortical bone in the midshaft of human femur and its correlation with CT scanning data. *Calcif Tissue Int* 2004; 74: 302–309.
16. Taddei F, Cristofolini L, Martelli S, et al. Subject-specific finite element models of long bones: an in vitro evaluation of the overall accuracy. *J Biomech* 2006; 39: 2457–2467.
17. Bergmann G, Deuretzbacher G, Heller M, et al. Hip contact forces and gait patterns from routine activities. *J Biomech* 2001; 34: 859–871.
18. Pettersen SH, Wik TS and Skallerud B. Subject specific finite element analysis of stress shielding around a cementless femoral stem. *Clin Biomech* 2009; 24: 196–202.
19. Ridzwan MIZ, Solehuddin Shuib, Hassan AY, et al. Optimization in implant topology to reduce stress shielding problem. *J Appl Sci* 2006; 6: 2768–2773.
20. Oh I-H, Nomura N, Masahashi N, et al. Mechanical properties of porous titanium compacts prepared by powder sintering. *Scripta Mater* 2003; 49: 1197–1202.
21. Laz PJ, Stowe JQ, Baldwin MA, et al. Incorporating uncertainty in mechanical properties for finite element-based evaluation of bone mechanics. *J Biomech* 2007; 40: 2831–2836.
22. Bendsøe MP and Sigmund O. Material interpolation schemes in topology optimization. *Arch Appl Mech* 1999; 69: 635–654.
23. Tensi HM, Gese H and Ascherl R. Non-linear three-dimensional finite element analysis of a cementless hip endoprosthesis. *Proc IMechE, Part H: J Engineering in Medicine* 1989; 203: 215–222.
24. Li W, Rungsiyakull C, Field C, et al. Computational biomechanics of bone's responses to dental prostheses – osseointegration, remodeling and resorption. *IOP Conf Ser Mater Sci Eng* 2010; 10: 12122.
25. Frost HM. A determinant of bone architecture. The minimum effective strain. *Clin Orthop Relat Res* 1983; 175: 286–292.
26. Duncan RL and Turner CH. Mechanotransduction and the functional response of bone to mechanical strain. *Calcif Tissue Int* 1995; 57: 344–358.

## Appendix I

### Notation

$E_b$	Young's modulus of bone
$E_l, E_u$	lower and upper limits of Young's modulus for the range of porosity considered in implant metal
$E^i$	Young's modulus of material in the elements belonging to the volume of $i$ th element set
$N$	number of element sets considered in optimization
$Vol^{element}$	element volume
$\epsilon$	effective strain
$\epsilon_1, \epsilon_2, \epsilon_3$	maximum, mid and minimum principal strain
$\rho_{app}$	apparent density of bone
$\rho^i$	volume fraction of material in the elements belonging to the volume of $i$ th element set
$\sigma_{y-min}$	yield point stress for implant metal corresponding to highest porosity
$\sigma^{element}$	von Mises stress at the centroid of the element

$\sigma_{vM}^i$	von Mises stress in the implant element/ element set $i$	$\tau_{avg}^{interface}$	average interfacial shear stress at implant and femur bone interface
$\sigma_{vM}^{pos-THR}$	volume average of von Mises stress for the elements in the ROI for the resected femur	$\tau_{max}$	maximum allowable value of interfacial shear stress at implant and femur bone interface
$\sigma_{vM}^{pre-THR}$	volume average of von Mises stress for the elements in the ROI for the intact femur		